Published in final edited form as:
Nat Genet. ; 44(8): 910–915. doi:10.1038/ng.2347.

FAN1 mutations cause karyomegalic interstitial nephritis, linking chronic kidney failure to defective DNA damage repair

Weibin Zhou[1,29], **Edgar A. Otto**[1,29], **Andrew Cluckey**[1], **Rannar Airik**[1], **Toby W. Hurd**[1], **Moumita Chaki**[1], **Katrina Diaz**[1], **Francis P. Lach**[2], **Geoffrey R. Bennett**[2], **Heon Y. Gee**[1], **Amiya K. Ghosh**[1], **Sivakumar Natarajan**[1], **Supawat Thongthip**[2], **Uma Veturi**[2], **Susan J. Allen**[1], **Sabine Janssen**[1], **Gokul Ramaswami**[1], **Joanne Dixon**[3], **Felix Burkhalter**[4], **Martin Spoendlin**[5], **Holger Moch**[6], **Michael J. Mihatsch**[7], **Jerome Verine**[8], **Richard Reade**[9], **Hany Soliman**[10], **Michel Godin**[11], **Denes Kiss**[12], **Guido Monga**[13,14], **Gianna Mazzucco**[15], **Kerstin Amann**[16], **Ferruh Artunc**[17], **Ronald C. Newland**[18], **Thorsten Wiech**[19], **Stefan Zschiedrich**[20], **Tobias B. Huber**[20,21], **Andreas Friedl**[22], **Gisela G. Slaats**[23], **Jaap A. Joles**[23], **Roel Goldschmeding**[24], **Joseph Washburn**[25], **Rachel H. Giles**[23], **Shawn Levy**[26], **Agata Smogorzewska**[2,30], and **Friedhelm Hildebrandt**[1,27,28,30]

[1]Department of Pediatrics, University of Michigan, Ann Arbor, Michigan 48109, USA [2]Laboratory of Genome Maintenance, The Rockefeller University, New York, NY, USA [3]Central & Southern Regional Genetic Service, Wellington Hospital, Wellington South, New Zealand [4]Transplantation Immunology and Nephrology, University Hospital Basel, Basel, Switzerland [5]Merian Iselin Klinik, CH-4054, Basel, Switzerland [6]Department of Pathology, University Hospital Zurich, Zurich, Switzerland [7]Pathology, University Hospital Basel, Basel, Switzerland [8]Université Paris Diderot, Sorbonne Paris Cité, Laboratoire de Pathologie, UMR-S 728, F-75010 Paris, France [9]Clinique Néphrologique du Pont Allant, Maubeuge, France [10]Assistance Publique–Hôpitaux de Paris, Hôpital Saint-Louis, Service de Biochimie, Paris, 75010, France [11]Department of Nephrology and

[30]Correspondence should be addressed to: Friedhelm Hildebrandt, M.D., Howard Hughes Medical Institute, University of Michigan Health System, 8220C MSRB III, 1150 West Medical Center Drive, Ann Arbor, MI 48109-5646, USA, Phone: +1 734 615-7285 (office), +1 734 615-7895, -7896 (laboratories); Fax: +1 734-615-1386, -7770, fhilde@umich.edu or: Agata Smogorzewska, M.D., Ph.D., Assistant Professor, Head, Laboratory of Genome Maintenance, Rockefeller University, 1230 York Avenue, New York, NY 10065-6399, Office phone: (212) 327-7850, Lab phone: (212) 327-8862, Fax: (212) 327-8262, asmogorzewska@rockefeller.edu.
[29]These authors contributed equally to this work.

ACCESSION NUMBERS

Human *FAN1*: NM_014967.4

AUTHOR CONTRIBUTIONS

W.Z. performed all zebrafish studies.
E.O., A.C., K.D., H.Y.G., T.W.H., M.C., A.G., S.N., S.J.A, S.J., G.R., and F.H. prepared and evaluated exome sequences. A.C. and F.H. identified the human *FAN1* gene mutation.
F.P.L performed the breakage and cell cycle analysis. A.S. and G.R.B. did western blotting in patient cell lines, A.S., G.R.B., and U.V. did sensitivity assays. S.T. performed epistasis analysis.
J.W. did genomic mapping. S.L. performed exome capture and massively-parallel sequencing.
R.A., T.W.H, M.C. and A.K.G, characterized antibodies. J.A.J., R.G. and R.H.G. performed γH2AX histochemistry.
A.C., K.D., J.D., F.B., M.S., H.M, M.J.M., A.F., J.V., R.R., H.S., M.G., D.K., G.M., K.A., F.A., R.C.N., T.W., S.Z., T.B.H., and F.H. recruited patients and gathered detailed clinical information for the study.
F.H. conceived of and directed the project and wrote the paper together with A.S.

COMPETING INTERESTS STATEMENT

The authors declare that they have no competing financial interests.

Hemodialysis, Rouen University Hospital, Rouen, France [12]Renal Division, Kantonsspital Liestal, Liestal, Switzerland [13]Department of Medical Sciences, Faculty of Medicine, University Amedeo Avogadro of the Eastern Piedmont, Novara, Italy [14]Department of Pathology, Maggiore della Carità Hospital, Novara, Italy [15]Department of Biomedical Sciences and Human Oncology, Faculty of Medicine, University of Torino, Italy [16]Nephropathology, Department of Pathology, University of Erlangen-Nürnberg, Germany [17]Department of Internal Medicine, Division of Nephrology, University Hospital Tübingen, D-72076 Tübingen, Germany [18]Department of Anatomical Pathology, Concord Hospital, Sydney, NSW, Australia [19]Institute of Pathology, University Hospital Freiburg, Freiburg, Germany [20]Renal Division, University Hospital Freiburg, Freiburg, Germany [21]BIOSS Centre for Biological Signalling Studies, Albert-Ludwigs-University Freiburg, Germany [22]Department of Pathology and Laboratory Medicine University of Wisconsin, Madison, Wisconsin USA [23]Department of Nephrology and Hypertension, University Medical Center, Utrecht, The Netherlands [24]Department of Pathology, University Medical Center Utrecht, The Netherlands [25]University of Michigan Comprehensive Cancer Center, University of Michigan, Ann Arbor, Michigan, USA [26]HudsonAlpha Institute for Biotechnology, 601 Genome Way, Huntsville, Alabama 35806, USA [27]Department of Human Genetics, University of Michigan, Ann Arbor, Michigan 48109, USA [28]Howard Hughes Medical Institute, Chevy Chase, MD, USA

SUMMARY

Chronic kidney disease (CKD) represents a major health burden[1]. Its central feature of renal fibrosis is not well understood. By whole exome resequencing in a model disorder for renal fibrosis, nephronophthisis (NPHP), we identified mutations of *Fanconi anemia-associated nuclease 1* (*FAN1*) as causing karyomegalic interstitial nephritis (KIN). Renal histology of KIN is indistinguishable from NPHP except for the presence of karyomegaly[2]. FAN1 has nuclease activity, acting in DNA interstrand crosslinking (ICL) repair within the Fanconi anemia pathway of DNA damage response (DDR)[3–6]. We demonstrate that cells from individuals with *FAN1* mutations exhibit sensitivity to the ICL agent mitomycin C. However, they do not exhibit chromosome breakage or cell cycle arrest after diepoxybutane treatment, unlike cells from patients with Fanconi anemia. We complement ICL sensitivity with wild type *FAN1* but not mutant cDNA from individuals with KIN. Depletion of *fan1* in zebrafish revealed increased DDR, apoptosis, and kidney cysts akin to NPHP. Our findings implicate susceptibility to environmental genotoxins and inadequate DNA repair as novel mechanisms of renal fibrosis and CKD.

Nephronophthisis (NPHP)-related ciliopathies are a heterogeneous group of recessive diseases that cause CKD by chronic fibrosis and cyst development in the kidney[7]. To identify additional causative genes for NPHP we performed homozygosity mapping[8] and whole exome resequencing[9] in two siblings (A1170) of Maori descent (Table 1). Renal histology was indistinguishable from NPHP except for enlarged nuclei as seen in karyomegalic interstitial nephritis (KIN)[10] (Figure 1). KIN is a kidney disease with renal tubular degeneration of unknown origin. It was first described in 1974[11] and given this term by Mihatsch et al[2]. KIN causes CKD on the basis of renal histologic changes characteristic for NPHP[2], which are tubular basement membrane degeneration, atrophic tubules, tubular microcysts, interstitial infiltrations, and pronounced fibrosis (Figure 1a)[12]. The only

distinguishing feature from NPHP in KIN is the presence of karyomegaly (Figure 1b–c), which can also be present in lung, liver, and brain[13]. Currently, 12 families with KIN have been described[10,14], compatible with autosomal recessive inheritance.

By homozygosity mapping in family A1170 we obtained 7 candidate regions of homozygosity by descent (Supplementary Figure 1A). Whole exome resequencing yielded a homozygous nonsense mutation (Trp707*) in *FAN1* (*Fanconi anemia-associated nuclease 1*) in both affected siblings (Supplementary Figure 1B, Table 1). No additional homozygous truncating mutations were detected in any other gene within the mapped candidate regions of A1170 (Supplementary Figure 1A). We then obtained DNA samples from 5 published KIN families and 5 unpublished cases (Table 1). Clinical phenotypes have been published for families A4385[15], A4393[16], A1170[10], A4433[13], and A4333[14] (Supplementary Table 1). Upon Sanger sequencing of all *FAN1* exons, we found 12 different mutations of *FAN1* in 9 of the 10 families with KIN (Supplementary Figure 1B, Table 1), detecting both mutated alleles in 9 families (Table 1). Eight of the 12 mutations truncated the conceptual reading frame (Table 1). Three missense mutations, Gln929Pro, Gly937Asp and Asp960Asn, concerned amino acid residues that are conserved throughout evolution and are positioned in the nuclease domain (VRR-NUC) of FAN1[6]. All mutations were absent from 96 healthy controls. We thus identified recessive mutations of *FAN1* as the cause of KIN, an NPHP-like fibrotic kidney disease.

FAN1 is considered an effector of the Fanconi anemia pathway, a DNA damage response signaling (DDR) pathway devoted to repair of DNA interstrand crosslink (ICL) damage[17]. Individuals with Fanconi anemia are characterized by developmental abnormalities, bone marrow failure, and predisposition to cancer[18]. However, no *FAN1* mutations were detected in Fanconi anemia individuals of unassigned complementation groups (F.P.L. and A.S., unpublished data). FAN1 is recruited to sites of ICL damage by interacting with a monoubiquitinated FANCI-FANCD2 (ID) complex through its UBZ domain[3–6]. *In vitro*, FAN1 exhibits nuclease activity.

We tested *FAN1* expression in fibroblasts and lymphoblastoid cell lines from individuals with KIN (Figure 2a). As predicted, no FAN1 protein was detected in the three individuals (A1170-22, A4385-22 and A4466-21) who had two truncating mutations of *FAN1* (Figure 2a and Supplementary Fig. 2). Conversely, the protein was detected in the cell line from individual A4486-23 with a missense mutation (Asp960Asn) in the nuclease domain of FAN1 (Figure 2a).

As depletion of *FAN1* sensitizes human cell lines to ICL agents[3–6], we then examined *FAN1*-mutant cells from individuals with KIN for genome instability upon treatment with mitomycin C (MMC) (Figure 2b and Supplementary Table 2). We observed chromatid breaks and radial chromosomes on metaphase spreads (Figure 2b), which is consistent with a role of FAN1 in genome maintenance and DDR. The levels of genome instability observed in KIN cell lines were not as high as in FA cell lines that lack *FANCA* gene function (RA3087 and RA3157), but were above background seen in wild type cells (Supplementary Table 2). Interestingly, the classic test for FA, diepoxybutane (DEB) breakage[19], was

negative in all *FAN1*-mutant cell lines tested but positive in the control *FANCA* mutant cell lines (RA3087 and RA3157) (Supplementary Table 2).

Despite the differences in apparent chromosomal instability following MMC and DEB treatment, survival of *FAN1*-mutant patient cell lines was severely compromised after treatment with either ICL agent (Figure 2c–f). ICL sensitivity was observed in multiple patient cell lines (Figure 2c–f). In contrast, cell cycle arrest in late S/G_2 phase, which is characteristic of Fanconi anemia cells, was seen in *FAN1*-mutant cells only after MMC and not after DEB treatment (Figure 2g). These observed differences between *FANCA* mutant and *FAN1* mutant cells might be explained by differential engagement of FAN1 *versus* other Fanconi anemia pathway-directed nucleases in the repair of different DNA ICL lesions, or by a different processing of the same kind of lesion by these distinct nucleases. Unlike the Fanconi anemia pathway defect, the FAN1 deficiency clearly results in high ICL sensitivity in the survival assays but does not lead to the profound genomic instability seen in Fanconi anemia cells. These differences in cellular phenotypes of *FAN1*-negative and *FANCA* negative cell lines may explain the lack of apparent phenotypic similarities between *FAN1*-negative individuals, who present with KIN, and FA individuals who have bone marrow failure and cancer predisposition. A differential phenotype is also consistent with our finding that FAN1 is not necessary for activation of the FA pathway, as judged by normal FANCD2 ubiquitination in *FAN1* negative cells (Supplementary Fig. 3).

To complement the *FAN1* defect, we transduced fibroblasts of individual A1170-22 with *FAN1* cDNA of, i) wild type, ii) mutations from patients with KIN, or iii) mutations known to inhibit the nuclease activity (Glu975AlaLys977Ala) or the interaction with FANCD2 (Cys44AlaCys47Ala)[6] (Figure 3a–b). No FAN1 protein was detected upon immunoblotting when expressing the two truncating mutations Trp707* and Arg679Thrfs*5 suggesting that they are unstable, while L925Profs*25 yielded a shortened protein product (Figure 3b). Whereas wild type *FAN1* did complement the MMC sensitivity defect, neither of the cDNAs representing mutations in individuals with KIN rescued the defect with the exception of Cys871Arg, which partially complemented cell survival upon MMC exposure, suggesting that it represents a hypomorphic allele of *FAN1* (Figure 3a). Interestingly, the *FAN1* mutation Cys44AlaCys47Ala that abolishes FANCD2-dependent localization of FAN1 to sites of DNA damage[6] was fully capable of rescuing the MMC resistance defect, strongly suggesting that FAN1 activity is independent of the FA pathway in cell lines from individuals with KIN. The Glu975AlaLys977Ala mutant lacking nuclease activity could not complement the *FAN1* defect.

It was previously shown in DT40 chicken cells that deletion of *FAN1* caused an effect on ICL sensitivity that was additive to the effect seen upon deletion of the Fanconi anemia genes *FANCC* and *FANCJ*[20]. To test whether inhibition of the Fanconi anemia pathway in the *FAN1*-mutant cells leads to increased ICL sensitivity, we depleted FANCD2, SLX4, or the SLX4-associated nucleases XPF and MUS81 (Figure 3c–d, Supplementary Fig. 4). Their depletion gave rise to profound MMC sensitivity that was greater than in cells with FAN1 deficiency alone, suggesting that FAN1 can work independently of the Fanconi Anemia pathway in repair of ICL damage.

The mechanisms that produce the fibrotic and cystic kidney phenotypes observed in NPHP-related ciliopathies are still mostly unknown[7,21,22]. Because most DDR pathways as well as NPHP-related ciliopathies phenotypes are conserved in zebrafish[23–27], we evaluated whether *FAN1* loss of function would cause both, disturbance of DDR signaling and NPHP-RC-like phenotypes by morpholino (MO) oligonucleotide knockdown of *fan1* in zebrafish embryos. Injection into 1–4 cell stage embryos of an MO (*fan1*D7) that targets the splice acceptor site of exon 7 (Supplementary Fig. 5A–C) caused the characteristic NPHP-like phenotype of shortened body axis (Fig. 4a–b), but also the DDR phenotypes of microcephaly, microphthalmia, and massive cell death throughout the embryo (Fig. 4c). Cell death was from apoptosis as demonstrated by activated caspase-3 (Fig. 4d and Supplementary Fig. 5D–E). DDR signaling was activated with increased signal of γH2AX upon immunofluorescence (Fig. 4e and Supplementary Fig. 5F–G). These finding are similar to the ones described upon knockdown of the Fanconi anemia gene *fancd2* in zebrafish[28,29]. However, in addition our *fan1*D7 MO morphants exhibited phenotypes characteristic of NPHP-related ciliopathies[27], including ventral body axis curvature and renal cysts, when apoptosis was suppressed through knockdown of p53 function (Fig. 4f–h). Specifically, zebrafish embryos injected with *fan1*D7 MO and p53 MO at 72 hpf displayed pronephric kidney cysts (19±3%) (Fig. 4f,h) and body curvature (not shown) (45±4%), whereas p53 MO alone did not cause pronephric cysts (Fig. 4g,h) and caused body axis curvature in a significantly smaller fraction of embryos (11±2%) (Fig. 4h). Thus, loss of *fan1* function results in ciliopathy-related phenotypes, which are further revealed when p53 function is inhibited. The masking of the renal cystic phenotype in the presence of p53 function is most likely due to the fact that *fan1* morphants exhibited embryonic deformity (Fig. 4b–c) and strongly elevated apoptosis (Fig. 4d and Supplementary Fig. 5D–E), which prevented the observation of kidney cysts that developed in later embryonic stages. Our data demonstrate that loss of *fan1* function in zebrafish embryos leads to a dual set of phenotypes, one representing activation of DDR and apoptosis (microcephaly and microphthalmia), the other mimicking NPHP-like ciliopathy phenotypes that are revealed when p53-dependent apoptosis is suppressed. Interestingly, we found that, while knockdown of *fancd2* in zebrafish led to increased γH2AX staining, it did not cause kidney cysts or other ciliopathy phenotypes seen in *fan1* knockdown (data not shown).

The clinical phenotypes in mutation of *FAN1 vs. FANCD2* differ significantly. The former causes KIN and histologic karyomegaly in liver and brain, whereas the latter causes Fanconi anemia. To evaluate whether these phenotypic differences can be partially attributed to differential tissue expression, we performed quantitative PCR of 48 different human tissue sources, showing significant differences of expression levels in 25 sources. Interestingly, *FAN1* expression exceeds *FANCD2* in parenchymatous organs including the kidney, liver, neuronal tissue and female reproductive organs (Fig. 5a), whereas *FANCD2* expression levels far exceed *FAN1* expression in 6 different lymphatic or bone marrow-derived sources as well as in skin and testis (Fig. 5b). This may partially explain why *FAN1* mutations cause KIN and karyomegaly in parenchymatous organs in the absence of Fanconi anemia-like blood dyscrasias, whereas *FANCD2* mutation causes Fanconi anemia, with pancytopenia, skin involvement and male infertility. Fan1 expression by western blotting was particularly

high in the kidney (Supplementary Fig. 6) suggesting that the kidney might depend on FAN1 for its normal function.

We recently identified two additional genes that play a role in DDR signaling as causing NPHP-related ciliopathies if mutated.[30] These findings strongly suggest that DDR may play a significant role in the pathogenesis of CKD in NPHP-related ciliopathies.

We therefore hypothesized that a defect in DDR signaling may represent a broader pathogenic mechanism that applies also to other forms of CKD. We therefore evaluated renal tissue sections from a standard congenic rat model for progressive chronic renal failure, the fawn-hooded hypertensive (FHH) rat, which has well-defined physiological parameters. Ten animals were selected based on disease progression at 9–10 months of age as measured by proteinuria.[31] To determine the load of DDR in kidneys of these animals, we applied the widely accepted criterion of increased nuclear γH2AX activation on immunohistochemistry as readout (Fig. 5c–e). After staining, whole slides (2–4 kidney sections per animal) were digitally scanned and 10 randomized cortical fields were analyzed per section for positive nuclei using a modified algorithm used and calibrated for diagnostic pathology. In total, between 2,000–3,000 cells were scored blindly per animal. A positive correlation (R^2=0.64, $p<0.0054$) was found between disease progression and DDR in this assay (Fig. 5c).

Having established the quantitative correlation in a well-defined congenic model for kidney disease we examined genetically heterogeneous human patients. A small pilot study using renal transplant biopsies from individuals clinically well-characterized by a nephropathologist and nephrologist supports the correlation found in the rat model. We examined γH2AX immunostaining of individuals four months post kidney transplantation with a histology report without injury and no proteinuria (Fig. 5f), a specimen from a transplant kidney 16 yrs after transplantation with (pathology report of “chronic damage”) (Fig. 5g), and a transplant kidney 10 years post-transplantation (pathology report of “chronic tissue damage”) (Fig. 5h). These data support in human CKD the relationship seen in the FHH rat model between the extent of kidney damage and DNA damage (γH2AX). They suggest that DDR may partially drive renal damage in pediatric NPHP-RC and in CKD of adults.

We here identify recessive mutations of *FAN1* as causing KIN, which causes CKD with fibrotic degeneration of the kidney. Thus, DDR, which plays a known role in cellular senescence[32] might contribute to the ‘premature aging’ phenotype of renal fibrosis in NPHP-like diseases. A KIN-like phenotype has also been described in humans and animal models that were exposed to ochratoxin A[15], busulfan or pyrrolizidine alkaloids[11], all of which cause DNA ICL. Thus, *FAN1* mutation represents the genetic equivalent of environmental genotoxic causes of KIN by the shared pathogenic mechanism of defective DNA ICL repair. In this context it is interesting to note that among the 12 individuals with KIN and *FAN1* mutations, CKD ensued by a median age at 45 years (Supplementary Table 1) and that 7 of the 12 KIN individuals carried two truncating mutations or missense mutations in the nuclease domain of *FAN1*, which most likely represent null alleles (Table 1, Fig. 3a). This raises the question, whether other individuals, who carry two hypomorphic

alleles rather than two null alleles, might develop end-stage kidney disease even later in life. Interestingly, a high percentage of adult individuals treated within chronic dialysis programs suffer from fibrotic nephropathy of unknown cause. We will therefore follow up on the hypothesis that a significant number of cases in this cohort might be caused by two hypomorphic alleles of *FAN1*. Furthermore, as we demonstrate here that recessive mutations of *FAN1* convey susceptibility to MMC and DEB, *FAN1* mutations may also sensitize to other DNA ICL causing environmental genotoxins such as ochratoxin A, which are abundant[16]. Because CKD always exhibits a histologic phenotype of chronic interstitial fibrosis similar to the one observed in KIN, it will be important to examine a potential role of ICL-causing genotoxins for the absolute and relative increase in end-stage kidney disease that has been observed over the last 20 years in developed countries[1].

ONLINE METHODS

Research subjects

We obtained blood samples and pedigrees following informed consent from individuals with KIN. Approval for human subjects research was obtained from the University of Michigan Institutional Review Board and the other institutions involved. The diagnosis of NPHP-RC was based on published clinical criteria. The clinical features of many individuals with KIN have been published (see also Table 1).[10,13–16,33]

Homozygosity mapping

For genome-wide homozygosity mapping[8] the 'Human Mapping 250k *Sty*I' array and the 'Genome-wide Human SNP 6.0 Array' from Affymetrix™ were utilized. Genomic DNA samples were hybridized, and scanned using the manufacturer's standard protocol at the University of Michigan Core Facility (www.michiganmicroarray.com). Non-parametric LOD scores were calculated using a modified version of the program GENEHUNTER 2.1[34,35] through stepwise use of a sliding window with sets of 110 SNPs using the program ALLEGRO.[36] Genetic regions of homozygosity by descent ('homozygosity peaks') were plotted across the genome as candidate regions for recessive disease-causing genes (see Fig. 1a), as described.[27,37] Disease allele frequency was set at 0.0001, and Caucasian marker allele frequencies were used.

Whole exome sequencing

Exome enrichment was conducted following the manufacturer's protocol for the 'NimbleGen™ SeqCap EZ Exome v2' beads (Roche NimbleGen Inc.). The kit interrogates a total of approximately 30,000 genes (~330,000 CCDS exons). Massively parallel sequencing was performed as described in Bentley et al.[38]

Mutation calling

Following whole exome sequencing, mutation calling was performed using the CLC Genomics Workbench™ software. Minimum length fraction of a read to match the reference sequence was set to 90%. For SNP detection, the minimum quality score of the central base and the minimum average quality score of surrounding bases were kept at default (20 and 15, respectively). Quality assessment was performed within a window of 11 bases. Only

reads which uniquely aligned to the reference genome were used for variant SNP or DIP (deletion/insertion polymorphism) calling. In patients with evidence of homozygosity by descent, the threshold for the number of reads (minor allele frequency) was set to >55%.

Filtering of variants from normal reference sequence (VRS)[27]

For deletions/insertions (DIPs) and single nucleotide polymorphisms (SNPs) we used the following *a priori* criteria to restrict the high number of VRS (average of 53,272 for DIPs and 315,372 for SNPs) as follows:

- **i.** We retained *exonic* variants (missense, nonsense, indels) and obligatory splice site variants only.
- **ii.** We included only VRSs that are not listed in the data base 'SNP129' of innocuous polymorphisms.
- **iii.** We evaluated exonic changes only within genomic regions, in which homozygosity mapping showed linkage for both affected siblings (retained average 38 for DIPs and 169 for SNPs).
- **iv.** Variants were analyzed using the program BLAT (http://genome.ucsc.edu/cgi-bin/hgBlat?command=start) at the UCSC human genome Bioinformatics Browser (http://genome.ucsc.edu/) for the presence of paralogous genes, pseudogenes, misalignments at ends of sequence reads, and whether the variant is a known dbSNP132 with an allele frequency >1% in Caucasian populations. In families in whom mapping demonstrated homozygosity by descent, we retained only homozygous variants and scrutinized all of them in the sequence alignments within CLC Genomics Workbench™ software for the presence of mismatches, indicating potential false alignments or poor sequence quality.
- **v.** Sanger sequencing was performed to confirm the remaining variants in original DNA samples and to test for intrafamilial segregation in a recessive mode.
- **vi.** Finally, remaining variants were ranked by the criteria whether mutations were truncating the conceptual reading frame (nonsense, frameshift and obligatory splice variants) or by evolutionary conservation analysis of missense variants, and by using web-based programs predicting the impact of disease candidate variants on the encoded protein or whether they were known disease-causing mutations.

Segregation analysis by Sanger sequencing

We applied Sanger dideoxy-terminator sequencing for confirmation and segregation of potential disease-causing variants in the respective patients, their affected siblings and their parents. In patients in whom only one heterozygous mutation was detected by exome capture and massively parallel sequencing, all exons and flanking intronic sequences of the respective gene(s) were analyzed by Sanger sequencing. Polymerase chain reaction (PCR) was performed using a touchdown protocol described previously.[39] Sequencing was performed using BigDye® Terminator v3.1 Cycle Sequencing Kit on an ABI 3730 XL sequencer (Applied Biosystem). Sequence traces were analyzed using Sequencher (version 4.8) software (Gene Codes Corporation).

Web-based variant analysis

Predictions on the possible impact of an amino acid substitution on the chemical change, evolutionary conservation, and protein function were obtained by using the following web-based programs: PolyPhen (Polymorphism Phenotyping, http://genetics.bwh.harvard.edu/pph/), PolyPhen2 (http://genetics.bwh.harvard.edu/pph2/), SIFT, (Sorting Intolerant from Tolerant, http://sift.jcvi.org/), and Mutation Taster (http://www.mutationtaster.org/). GERP calculation was performed using http://gvs.gs.washington.edu/SeattleSeqAnnotation/.

Cell culture

Human fibroblasts cells were grown in 3% oxygen in Dulbecco Modified Eagle medium (DMEM) supplemented with 15% (v/v) FBS, 100 units of penicillin per ml, 0.1 mg streptomycin per ml, and non-essential amino acids (all from Invitrogen). BJ cells are normal foreskin fibroblasts and were obtained from ATCC. Fibroblasts were immortalized using pWZLhTERT or/and pMSCVNeo HPV16E6E7. Lymphoblast cell lines (LCLs) were immortalized using EBV and were grown in RPMI supplemented as above except with 20% FBS.

DNA damage sensitivity assay

Cells were plated in a 6-well plate in triplicate at a density of 5×10^4 cells per well for primary fibroblasts and LCLs or 2.5×10^4 cells per well for transformed fibroblasts. Immediately after plating for LCLs, or 24 hours later for fibroblasts, MMC or DEB was added at a final concentration from 0 to 100 nM for MMC or 1–0.75 μg/ml for DEB. After 6 to 8 days in culture, cell numbers were determined using a Z2 Coulter Counter (Beckman Coulter). The cell number after MMC or DEB treatment was normalized to the cell number in the untreated sample to arrive at the % survival.

RNAi

For siRNA experiments, A1170-22 E6E7/hTERT cells were transfected with a pool of three siRNAs using Lipofectamine RNAiMAX (Invitrogen) according to the manufacturer's instruction with the final concentration of total siRNA at 25 nM. siRNA sequences are shown in Supplementary Table 3.

Mutagenesis

Mutagenesis of *FAN1* was performed on a pDONR223 *FAN1*[6] using multisite mutagenesis kit (Agilent). Primer sequences are shown in Supplementary Table 3. Other *FAN1* mutants were described in[6].

Antibodies

FAN1 antibody (RC394) was raised in a rabbit using GST-FAN1aa1-90 as an antigen and affinity-purified against HIS-FAN1aa1-90. Commercial antibodies were as follows: HA (Covance, MMS-101R), XPF/ERCC4 (Bethyl Laboratory, A301-315A), MUS81 (Sigma, M1445), FANCD2 (Novus, NB100-182).

Breakage analysis

Cells were treated with 0.01 or 0.1 μg Diepoxybutane (DEB) per mL of media for 72 h or with 50 nM MMC for 24 h, arrested with colcemid (0.167 microgram per mL of media) for 2 hours, harvested, incubated for 10 min at 37°C in 0.075 M KCl, and fixed in freshly prepared methanol:glacial acidic acid (3:1 v/v). Cells were stored at 4°C and when needed dropped onto wet slides and air-dried at 40°C for 60 minutes before staining with Karyomax Giemsa (Invitrogen) Gurr Buffer for 3 minutes. After rinsing with fresh Gurr Buffer followed by distilled water, the slides were fully dried at 40°C for 60 minutes and scanned using the Metasystems Metafer application.

Cell cycle analysis

Cells were left untreated, were treated with 100 nM MMC and grown for 48 hours, or were treated with 0.1 μg of Diepoxybutane (DEB) per ml and grown for 72 hours. Collected cells were resuspended in 300 μl PBS. While vortexing, 700 μl of ice cold 100% (v/v) ethanol was added dropwise, and the suspension was stored at −20°C at least overnight. Thirty minutes before fluorescence-activated cell sorting (FACS), cells were spun down, resuspended in propidium iodine mix (1 ml PBS, 10 μl RNase (of stock solution of 20 mg/ml), 10 ml propidium iodine (of stock solution of 1 mg/ml)) and analyzed using FACSCalibur (Becton Dickinson). Cell cycle analysis was performed using the FlowJo software (Tree Star, Inc).

fan1 zebrafish morpholino oligo-mediated knockdown

Morpholino oligonucleotides (MO) were obtained from Gene Tools, LLC (Philomath, OR). MO (*fan1*D7 at 0.1 mM, standard control at 0.2 mM, and *p53* MO at 0.2 mM) were injected into zebrafish embryos at 1–4 cell stages. Embryos were then fixed at 27 hpf with 4% PFA/PBS +1% DMSO overnight, permeablized with acetone at −20°C for 7 minutes, and stained with antibody against phosphorylated zebrafish γH2AX (1:1,000, gift from Amatruda lab at UT Southwestern, or antibody against cleaved Caspase-3 (1:200, BD Biosciences). Alex568-anti rabbit IgG was used at 1:2,000 and 1:1,000, respectively. The IF procedure followed standard protocol. After washing off secondary antibody, embryos were mounted in Vector-Shield Mounting Media and imaged with a Leica SP5X confocal system. Z-stacks were processed to reduce noise and overlayed to show the representative images of IF staining for γH2AX and cleaved caspase. DAPI was used to stain nuclei. Sequence of *fan1*D7 MO sequences is shown in Supplementary Table 3.

Quantitative real-time PCR

cDNAs of 48 human tissues were purchased from OriGene (Tissue SCANTM Normal Tissue qPCR Arrays cat. # HMRT502). Quantitative real-time PCR was performed using the TaqMan Gene Expression Assay Kit (Applied Biosystems) according to the manufacturer's instructions. Briefly, 1 μL of cDNA was mixed with 10 μL of 2X TaqMan Universal Master Mix and 1 μL of the 20X TaqMan Gene Expression Assay, and was brought to a total volume of 20 μL by using RNase-free water. Target amplification was performed in 96-well plates using the StepOnePlusTM Real-Time PCR System (Applied Biosystems). TaqMan probes for *FAN1* (Hs00429686_m1), *FANCD2* (Hs00276992_m1), and *glyceraldhyde-3-*

phosphate dehydrogenase (*GAPDH*) (Hs02758991_g1) were purchased from Applied Biosystems. PCR thermal cycling conditions included an initial 10 minutes hold at 95°C to activate the AmpliTaq Gold DNA polymerase, followed by 40 cycles of denaturation (15 seconds at 95°) and annealing/primer extension (15 seconds at 60°C). More than triplicate real-time RT-PCR analyses were executed for each sample and the obtained threshold cycle values were averaged. The relative RNA expression levels were calculated via a comparative threshold cycle (Ct) method using *GAPDH* as control: ΔCt=Ct(*GAPDH*)-Ct(*FAN1* or *FANCD2*). The gene expression fold change, normalized to the *GAPDH* and relative to the control sample (*FAN1* expression in the kidney), was calculated as $2^{-\Delta\Delta Ct}$.

Immunocytochemistry in the Fawn-Hooded Hypertensive rat and humans with kidney disease

Kidney tissue coupes of Fawn-Hooded Hypertensive rats (n=10) [31,40] embedded in paraffin were deparafinized and treated with PO block for 15 minutes and incubated at 100 °C in Citrate/HCL buffer for 20 minutes. The coupes were stained with mouse anti-γH2AX (1:200) overnight at 4°C. Polyclonal rabbit anti-mouse HRP (Dako, P0260) (1:100) was incubated 30 minutes at RT. Finally, BrightVision Poly HRP-Anti Rabbit IgG (Immunologic, DPVR55HRP) was incubated for 1 hour RT. Nova RED substrate kit for Peroxidase (Vector, SK-4800) was used and counterstained with hematoxyline. Analysis was performed using the Aperio ImageScope software. Ten random tubular fields in the cortex (approximately 270 cells per field) were analyzed for positive stained nuclei using an in-house algorithm macro. GraphPad Prism 5.0 was used to calculate the R square and p-value.

Statistical analysis

Student's two-tailed nonpaired *t*-tests and normal distribution two-tailed *z*-tests were carried out using pooled standard error and s.d. values to determine the statistical significance of different cohorts.

Bioinformatics

Genetic location is according to the March 2006 Human Genome Browser data (http://www.genome.ucsc.edu).

Supplementary Material

Refer to Web version on PubMed Central for supplementary material.

Acknowledgments

We are grateful to the families and study individuals for their contribution. We thank Dr. Arnaud Francois (Rouen) for contribution of pathology data and Dr. James Amatruda (Dallas) for antibodies. This research was supported by grants from the National Institutes of Health to F.H. (DK068306 and DK090917) and W.Z. (DK091405), by the Burroughs Wellcome Fund Career Award for Medical Scientists and the Doris Duke Charitable Foundation Clinical Scientist Development Awards to A.S. A.S. is a Rita Allen Foundation and an Irma T. Hirschl scholar.

F.H. is an Investigator of the Howard Hughes Medical Institute, a Doris Duke Distinguished Clinical Scientist, and a Frederick G. L. Huetwell Professor.

This work utilized two Cores of the Michigan Diabetes Research and Training Center funded by DK020572 from the National Institute of Diabetes and Digestive and Kidney Diseases.

References

1. Coresh J, Astor BC, Greene T, Eknoyan G, Levey AS. Prevalence of chronic kidney disease and decreased kidney function in the adult US population: Third National Health and Nutrition Examination Survey. Am J Kidney Dis. 2003; 41:1–12. [PubMed: 12500213]
2. Mihatsch MJ, et al. Systemic karyomegaly associated with chronic interstitial nephritis. A new disease entity? Clin Nephrol. 1979; 12:54–62. [PubMed: 527271]
3. Kratz K, et al. Deficiency of FANCD2-associated nuclease KIAA1018/FAN1 sensitizes cells to interstrand crosslinking agents. Cell. 2010; 142:77–88. [PubMed: 20603016]
4. Liu T, Ghosal G, Yuan J, Chen J, Huang J. FAN1 acts with FANCI-FANCD2 to promote DNA interstrand cross-link repair. Science. 2010; 329:693–696. [PubMed: 20671156]
5. MacKay C, et al. Identification of KIAA1018/FAN1, a DNA repair nuclease recruited to DNA damage by monoubiquitinated FANCD2. Cell. 2010; 142:65–76. [PubMed: 20603015]
6. Smogorzewska A, et al. A genetic screen identifies FAN1, a Fanconi anemia-associated nuclease necessary for DNA interstrand crosslink repair. Mol Cell. 2010; 39:36–47. [PubMed: 20603073]
7. Hildebrandt F, Benzing T, Katsanis N. Ciliopathies. N Engl J Med. 2011; 364:1533–1543. [PubMed: 21506742]
8. Hildebrandt F, et al. A Systematic Approach to Mapping Recessive Disease Genes in Individuals from Outbred Populations. PloS Genetics. 2009; 5:31000353.
9. Otto EA, et al. Candidate exome capture identifies mutation of SDCCAG8 as the cause of a retinal-renal ciliopathy. Nat Genet. 2010; 42:840–850. [PubMed: 20835237]
10. Palmer D, Lallu S, Matheson P, Bethwaite P, Tompson K. Karyomegalic interstitial nephritis: a pitfall in urine cytology. Diagn Cytopathol. 2007; 35:179–182. [PubMed: 17304531]
11. Burry AF. Extreme dysplasia in renal epithelium of a young woman dying from hepatocarcinoma. J Pathol. 1974; 113:147–150. [PubMed: 4372331]
12. Zollinger HU, et al. Nephronophthisis (medullary cystic disease of the kidney). A study using electron microscopy, immunofluorescence, and a review of the morphological findings. Helv Paediatr Acta. 1980; 35:509–530. [PubMed: 7009503]
13. Spoendlin M, et al. Karyomegalic interstitial nephritis: further support for a distinct entity and evidence for a genetic defect. Am J Kidney Dis. 1995; 25:242–252. [PubMed: 7847351]
14. Baba F, Nanovic L, Jaffery JB, Friedl A. Karyomegalic tubulointerstitial nephritis--a case report. Pathol Res Pract. 2006; 202:555–559. [PubMed: 16678356]
15. Godin M, et al. Karyomegalic interstitial nephritis. Am J Kidney Dis. 1996; 27:166. [PubMed: 8546134]
16. Verine J, Reade R, Janin A, Droz D. Karyomegalic interstitial nephritis: A new French case. Ann Pathol. 2010; 30:240–242. [PubMed: 20621605]
17. Knipscheer P, et al. The Fanconi anemia pathway promotes replication-dependent DNA interstrand cross-link repair. Science. 2009; 326:1698–1701. [PubMed: 19965384]
18. Auerbach AD. Fanconi anemia and its diagnosis. Mutat Res. 2009; 668:4–10. [PubMed: 19622403]
19. Auerbach AD, Wolman SR. Susceptibility of Fanconi's anaemia fibroblasts to chromosome damage by carcinogens. Nature. 1976; 261:494–496. [PubMed: 934283]
20. Yoshikiyo K, et al. KIAA1018/FAN1 nuclease protects cells against genomic instability induced by interstrand cross-linking agents. Proc Natl Acad Sci U S A. 2010; 107:21553–21557. [PubMed: 21115814]
21. Simons M, et al. Inversin, the gene product mutated in nephronophthisis type II, functions as a molecular switch between Wnt signaling pathways. Nat Genet. 2005; 37:537–543. [PubMed: 15852005]
22. Huangfu D, et al. Hedgehog signalling in the mouse requires intraflagellar transport proteins. Nature. 2003; 426:83–87. [PubMed: 14603322]

23. Otto EA, et al. Mutations in INVS encoding inversin cause nephronophthisis type 2, linking renal cystic disease to the function of primary cilia and left-right axis determination. Nat Genet. 2003; 34:413–420. [PubMed: 12872123]
24. Zhou W, Dai J, Attanasio M, Hildebrandt F. Nephrocystin-3 is required for ciliary function in zebrafish embryos. Am J Physiol Renal Physiol. 2010; 299:F55–62. [PubMed: 20462968]
25. Schafer T, et al. Genetic and physical interaction between the NPHP5 and NPHP6 gene products. Hum Mol Genet. 2008; 17:3655–3662. [PubMed: 18723859]
26. Sayer JA, et al. The centrosomal protein nephrocystin-6 is mutated in Joubert syndrome and activates transcription factor ATF4. Nat Genet. 2006; 38:674–681. [PubMed: 16682973]
27. Otto EA, et al. Candidate exome capture identifies mutation of SDCCAG8 as the cause of a retinal-renal ciliopathy. Nat Genet. 2010; 42:840–850. [PubMed: 20835237]
28. Liu TX, et al. Knockdown of zebrafish Fancd2 causes developmental abnormalities via p53-dependent apoptosis. Dev Cell. 2003; 5:903–914. [PubMed: 14667412]
29. Zeng Z, Richardson J, Verduzco D, Mitchell DL, Patton EE. Zebrafish have a competent p53-dependent nucleotide excision repair pathway to resolve ultraviolet B-induced DNA damage in the skin. Zebrafish. 2009; 6:405–415. [PubMed: 20047468]
30. Chaki M, Airik R. Exome capture reveals ZNF423 and CEP164 mutations, linking renal ciliopathies to DNA damage response signaling. Cell. 2012 in press.
31. Koeners MP, Braam B, van der Giezen DM, Goldschmeding R, Joles JA. A perinatal nitric oxide donor increases renal vascular resistance and ameliorates hypertension and glomerular injury in adult fawn-hooded hypertensive rats. Am J Physiol Regul Integr Comp Physiol. 2008; 294:R1847–1855. [PubMed: 18417652]
32. Mallette FA, Ferbeyre G. The DNA damage signaling pathway connects oncogenic stress to cellular senescence. Cell Cycle. 2007; 6:1831–1836. [PubMed: 17671427]
33. Moch H, Spondlin M, Schmassmann A, Mihatsch MJ. Systemic karyomegaly with chronic interstitial nephritis. Discussion of the disease picture based on an autopsy case. Pathologe. 1994; 15:44–48. [PubMed: 8153075]
34. Kruglyak L, Daly MJ, Reeve-Daly MP, Lander ES. Parametric and nonparametric linkage analysis: a unified multipoint approach. Am J Hum Genet. 1996; 58:1347–1363. [PubMed: 8651312]
35. Strauch K, et al. Parametric and nonparametric multipoint linkage analysis with imprinting and two-locus-trait models: application to mite sensitization. Am J Hum Genet. 2000; 66:1945–1957. [PubMed: 10796874]
36. Gudbjartsson DF, Jonasson K, Frigge ML, Kong A. Allegro, a new computer program for multipoint linkage analysis. Nat Genet. 2000; 25:12–13. [PubMed: 10802644]
37. Hildebrandt F, et al. A systematic approach to mapping recessive disease genes in individuals from outbred populations. PLoS Genet. 2009; 5:e1000353. [PubMed: 19165332]
38. Bentley DR, et al. Accurate whole human genome sequencing using reversible terminator chemistry. Nature. 2008; 456:53–59. [PubMed: 18987734]
39. Otto EA, et al. Mutation analysis in nephronophthisis using a combined approach of homozygosity mapping, CEL I endonuclease cleavage, and direct sequencing. Hum Mutat. 2008; 29:418–426. [PubMed: 18076122]
40. Koeners MP, Braam B, van der Giezen DM, Goldschmeding R, Joles JA. Perinatal micronutrient supplements ameliorate hypertension and proteinuria in adult fawn-hooded hypertensive rats. Am J Hypertens. 2010; 23:802–808. [PubMed: 20360751]

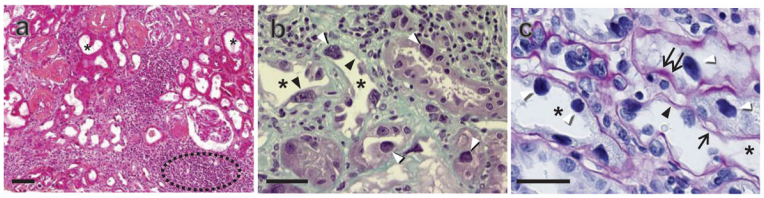

Figure 1. Renal histology in individuals with karyomegalic interstitial nephritis (KIN)

Renal histology of individuals with *FAN1* mutation exhibits the characteristic triad of nephronophthisis (NPHP), with cystic dilation of renal tubules (asterisks), interstitial infiltrations (encircled with a dotted line in **a**), and widespread fibrosis (blue-grey coloring in Trichrome-Masson staining in **b**). Karyomegaly is observed (white arrow heads in **b** and **c**) in tubules that have lost epithelial cells at their circumference (black arrow heads in **b** and **c**). The tubular basement membrane is thickened (double arrows in **c**) as well as attenuated (black arrow in **c**). **a** and **b** are from individual A4393-21, **c** is from individual A4466-21. Scale bars denote 100 μm.

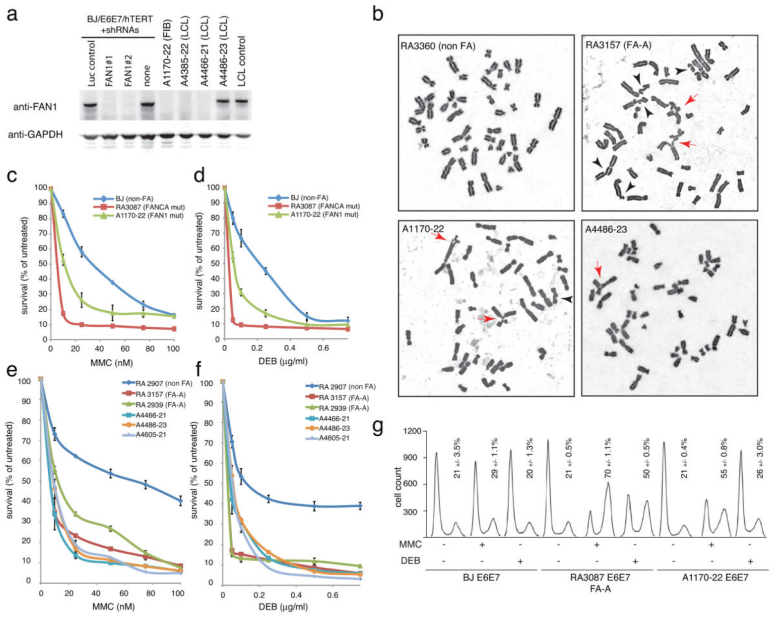

Figure 2. Phenotypes of *FAN1*-mutant cells

(**a**) Western blot analysis with anti-FAN1 antibody raised against the N-terminal 90 amino acids of FAN1. Specificity of the antibody was confirmed by the abrogation of signal after transduction of BJ fibroblasts with shRNAs against *FAN1* and in individuals with protein truncating mutations in *FAN1* (see Table 1). (**b**) Examples of metaphases of the indicated cell lines after treatment with 50 nM mitomycin C (MMC). Arrows indicate radial chromosomes, arrowheads indicate chromatid breaks. (**c**–**f**) MMC and diepoxybutane (DEB) sensitivity of the indicated *FAN1*-mutant cell lines in comparison to *FANCA* mutant and wild type cell lines. Primary fibroblast (FIB) (**c** and **d**) or lymphoblastoid cell lines (LCL) (**e** and **f**) were treated in triplicate with increasing levels of indicated DNA ICL inducing agent. After 6 or 8 days, cell numbers were determined using a Coulter counter. Total cell numbers at each dose were divided by the number of cells in the initial untreated sample to arrive at percent survival. Error bars indicate standard deviations. (**g**) Cell cycle analysis of the indicated fibroblast cell lines after treatment with 100 nM MMC or 0.1 µg of DEB per ml of media. Untreated samples were analyzed in parallel.

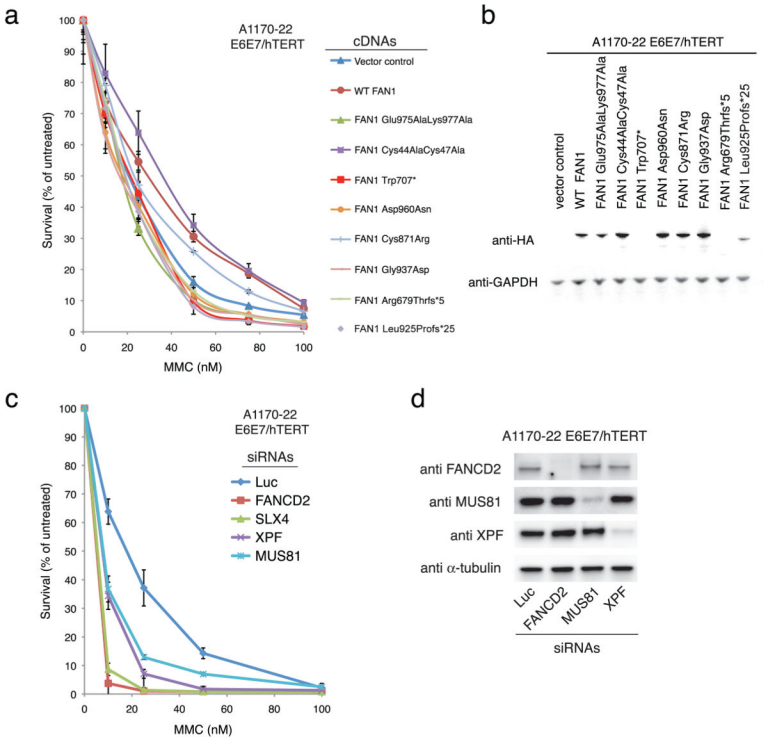

Figure 3. Complementation of *FAN1*-mutant cells with *FAN1* cDNAs, and epistasis analysis with genes implicated in ICL resistance

(**a**) Complementation of MMC sensitivity in fibroblasts of KIN individual A1170-22. Fibroblasts stably transduced with empty vector (vector control), vector expressing wild type *FAN1* cDNA, or *FAN1* cDNA with mutations incorporated (see Table 1) were exposed to different levels of MMC ranging from 0–100 nM. After 8 days, the cell number was determined using a Coulter counter. Total cell numbers at each dose were divided by the number of cells in the initial untreated sample to arrive at percent survival. Error bars indicate s.d. (**b**) Immunoblot showing expression levels of *FAN1* alleles in A1170-22 fibroblasts used in the MMC sensitivity assay shown in panel **a**. Note that Trp707* and Arg679Thrfs*5 lack expression of FAN1 and Leu925Profs*25 results in a shortened product. (**c**) MMC sensitivity in A1170-22 fibroblasts transfected with the indicated siRNAs. (**d**) Immunoblot of expression levels of indicated proteins after siRNA-mediated depletion in the A1170-22 fibroblasts used in the experiment shown in panel **c**.

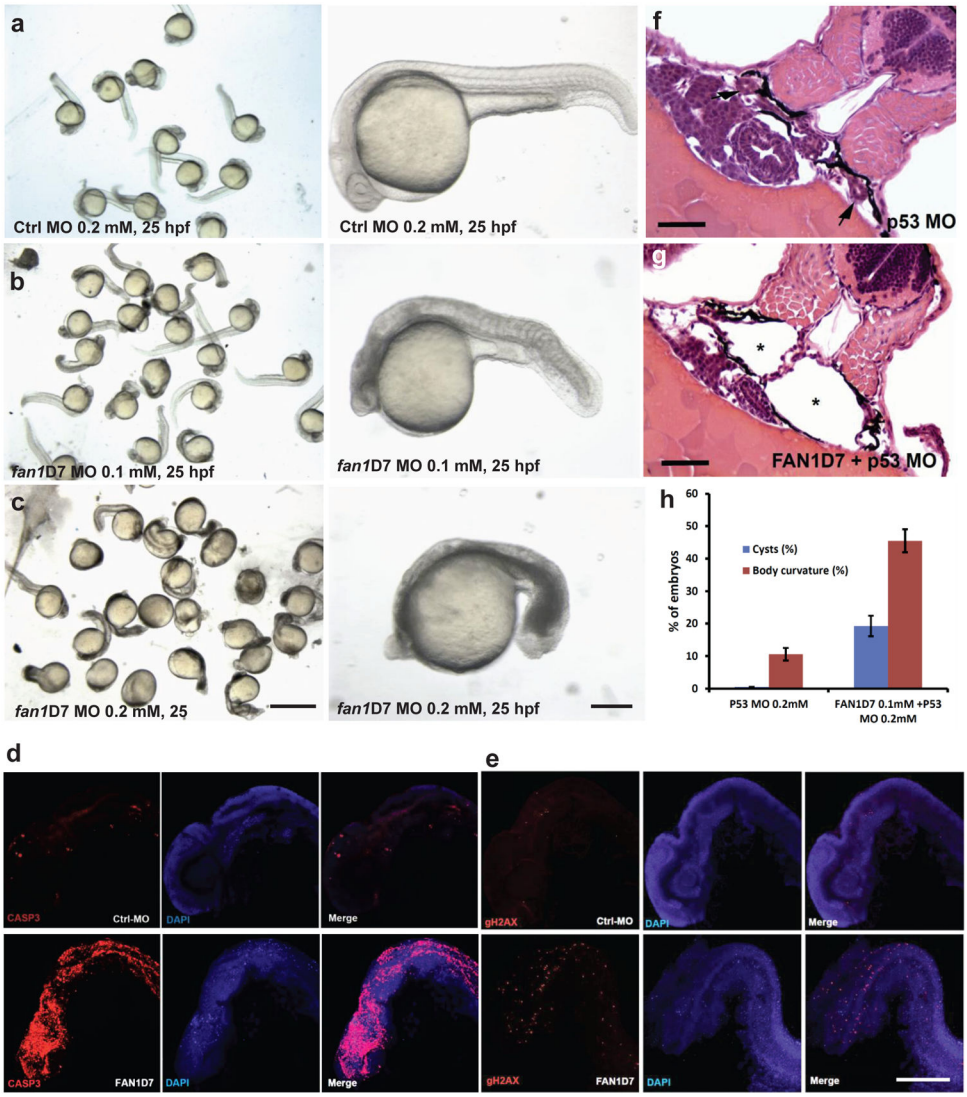

Figure 4. Phenotype of *fan1* loss of function in zebrafish

(**a**–**c**) Knockdown of *fan1* in zebrafish causes developmental abnormalities. A *fan1*D7 morpholino (MO) that targets the splice acceptor site of exon 7 (Supplementary Fig. 5) was injected into 1–4 cell stage embryos at the concentrations shown. Standard control MO (Ctrl) was injected at 0.2 mM. At 25 hpf (**b**–**c**), morphant embryos displayed shortened body axis, ventral body axis curvature, and massive cell death (dark grey tissue areas) throughout the embryo (see **c**), when compared to control MO (**a**). Scale bar in **a**–**c** is 750 μm for left panels and 150 μm for right panels.

(**d**–**e**) Knockdown of *fan1* in zebrafish induces widespread apoptosis. Upon *fan1* knockdown, utilizing *fan1*D7 MO as in (**a**–**c**), widespread apoptosis was seen in the anterior body (**d**) and the tail (Supplementary Fig. 5) of 27 hpf zebrafish, as detected by an antibody against activated caspase-3 (CASP3) compared to negative control morpholino. Images are representative for 32 embryos evaluated for control and MO knockdown, respectively. (**e**) Knockdown of *fan1* leads to increased staining with γH2AX antibody, indicating increased DDR. In knockdown embryos, 24 out of 27 embryos had elevated Caspase-3 staining, and

27 of 32 embryos stained with γH2AX had elevated expression of γH2AX. Scale bar is 250 μm. (See also Supplementary Fig. 5.)

(**f**–**h**) Knockdown of *fan1* on the background of p53 morphants reveals pronephric cysts. (**f**) *p53* knockdown alone does not cause pronephric cysts in 72 hpf embryos exhibiting normal pronephric tubules (arrows). (**g**) However, 72 hpf zebrafish embryos co-injected with *fan1D7* MO (0.1 mM) and *p53* MO (0.2 mM) display pronephric kidney cysts (19±3%) (asterisks in **g**) and results in body axis curvature (not shown) (45±4%). (**g**–**h**) it causes body axis curvature in a significantly smaller fraction (11±2%; not shown). Scale bar is 50 μm.

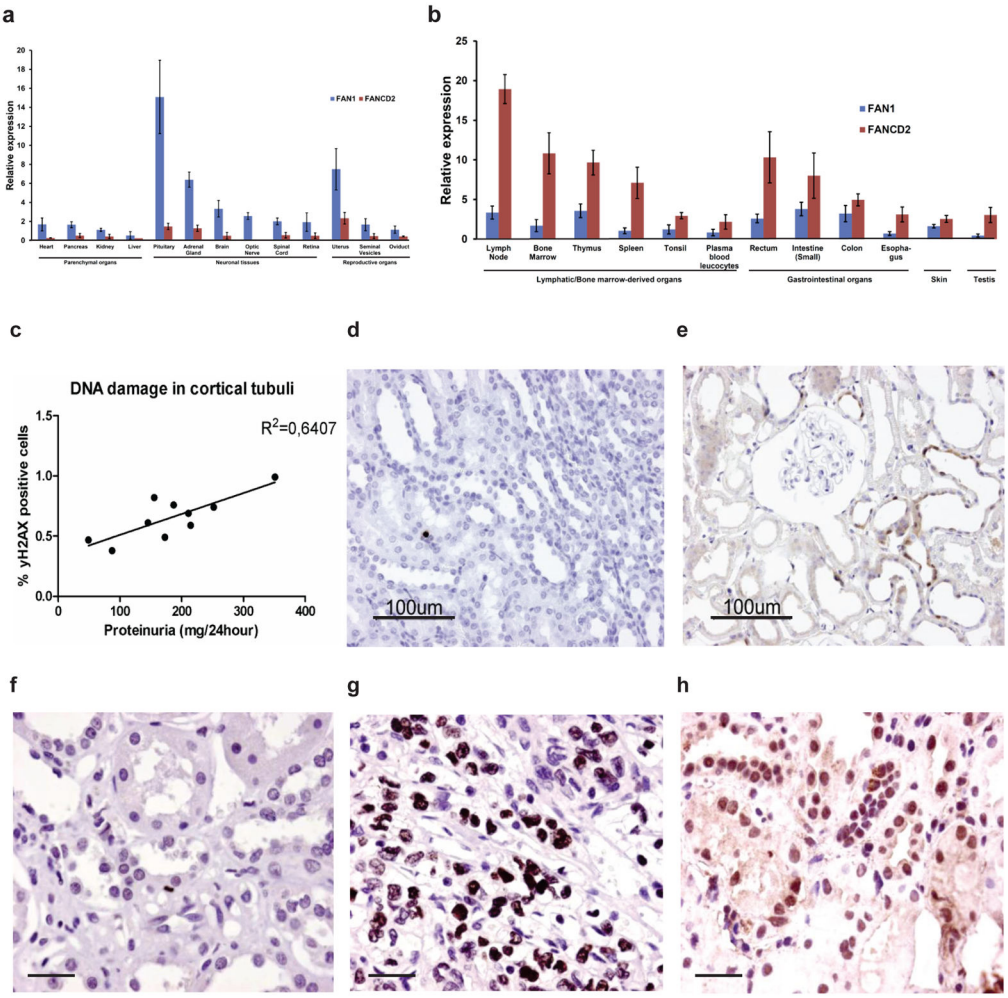

Figure 5. Differential expression levels of *FANCD2 vs. FAN1* in human tissue sources and increased DNA damage response in chronic kidney disease

Expression levels measured by quantitative real-time PCR were normalized against *GAPDH* expression. Error bars show SEM of triplicates.

(**a**–**b**) Expression levels of *FANCD2 vs. FAN1* in 25 different human tissue sources (of 48 total with differential expression). (**a**) *FAN1* expression exceeded *FANCD2* in parenchymatous organs including kidney, liver, neuronal tissue and female reproductive organs, whereas (**b**) *FANCD2* expression exceeds *FAN1* expression in lymphatic or bone marrow-derived sources, skin and testis.

(**c**–**h**) DNA damage response is pronounced in chronic kidney disease.

(**c**) Quantified percent of γ-H2AX staining of fawn-hooded hypertensive rat kidneys (between 2,000–3,000 cells scored per animal) with progressive kidney injury[31] correlates with proteinuria ($p<0.0054$).

(**d**) Example of γ-H2AX immunostaining in normal rat kidney.

(**e**) Example of chronically damaged kidney in the fawn hooded hypertensive rat.

(**f**–**h**) γ-H2AX staining of human kidney transplant biopsies: Transplant kidney, 4 months post-transplantation, no evidence for injury (**f**); transplant kidney, 16 yrs after

transplantation, chronic damage (**g**); transplant kidney with chronic tissue damage, 10 years post-transplantation (**h**). Scale bars in **d**–**h** are 100 μm.

Nat Genet. Author manuscript; available in PMC 2013 February 01.

Table 1

Mutations of *FAN1* in 9 families with karyomegalic interstitial nephritis.

Family-Individual	Ethnic origin	Nucleotide alteration[a,b]	Deduced protein change	Exon/Intron (state)	Continuous amino acid sequence conservation	Parental consan-guinity
A4385 -21 (no DNA) -22	French	c.1234+2T>A c.2036_7delGA	Splice site p.Arg679Thrfs*5	2 (het) 7 (het)	N/A N/A	No
A4466 -21	French	c.1234+2T>A c.2245C>T	Splice site p.Arg749*	2 (het) 9 (het)	N/A N/A	No
A4393 -21	French	c.1375+1G>A c.2616delA	Splice site p.Asp873Thrfs*17	3 (het) 12 (het)	N/A N/A	No
A4605 -21	German	c.1606C>T c.2786A>C	p.Arg536* p.Gln929Pro	5 (het) 12 (het)	N/A *D. rerio*[c]	No
A4486 -22 -23	German	c.1606C>T c.2878G>A	p.Arg536* p.Asp960Asn	5 (het) 13 (het)	N/A *S. pombe*[c]	No
A1170 -22 -25	New Zealand Maori	c.2120G>A	p.Trp707*	8 (hom)	N/A	distant?
A4433 -21	Spanish	c.2616delA	p.Asp873Thrfs*17	12 (hom)	N/A	No
A4407 -24	Swiss	c.2611T>C c.2878G>A	p.Cys871Arg p.Asp960Asn	12 (het) 13 (het)	(never “R”)[d] *S. pombe*[c]	No
A4333 -21	ND	c.2774_5delTT c.2810G>A	p.Leu925Profs*25 p.Gly937Asp	12 (het) 13 (het)	N/A *C. intestinalis*[c]	No

[a] Four different European founder mutations are underlined.

[b] *FAN1* cDNA mutations are numbered according to human cDNA reference sequence NM_014967.4, where +1 corresponds to the A of ATG start translation codon. First exon is non-coding.

[c] Amino acid residue is continually conserved throughout evolution, including *Danio rerio*, *Saccharomyces pombe*, or *Ciona intestinalis*, as indicated.

[d] Amino acid residue is not conserved in evolution, but never substituted by an “R”.

hom, homozygous; het, heterozygous; N/A, not applicable; ND, no data